CHAPTER IX.F

REACTION RATES AND KINETICS OF THE FISCHER-TROPSCH SYNTHESIS OVER AN IRON-BASED CATALYST

ABSTRACT

The kinetics of the Fischer-Tropsch synthesis and the water gas shift reaction has been obtained for an iron-based catalyst promoted with silica and potassium in a slurry phase reactor. Conversions, partial pressures and reaction rates were evaluated over a wide range of space velocities at 270°C, 1308 kPa and an inlet H_2/CO ratio of 0.67. The fraction of CO converted to produce hydrocarbons decreases with space time/conversion. This indicates that it would be beneficial, from a catalyst productivity viewpoint, to conduct the Fischer-Tropsch synthesis at intermediate conversion levels (per pass) with recycle or a series of reactors to achieve high conversions. The partial pressure of water is low at all the space velocities studied, and decreases at high synthesis gas conversion levels. The reaction rate expression for the conversion of synthesis gas that was developed ($-r_{CO+H_2} = kP_{CO}P_{H_2}/(1+K_{CO}P_{CO})$) shows negligible inhibition of the rate by the reaction products.

INTRODUCTION

The Fischer-Tropsch Synthesis consists of the conversion of synthesis gas (a mixture of carbon monoxide and hydrogen) to hydrocarbons. Recently there has been a resurgence of interest in Fischer-Tropsch synthesis, and particularly in the use of slurry reactors. These reactors offer considerable advantages over more conventional reactors including the ability to effectively manage the highly exothermic

reactions and to use directly synthesis gas with low H_2/CO ratio produced by advanced gasification processes without excessive catalyst coking (IX.F-1).

A number of transition metals are active catalysts for the Fischer-Tropsch synthesis. Iron-based catalysts are particularly attractive as they are inexpensive and are active for the water gas shift reaction allowing for the use of synthesis gas with a low H_2/CO ratio (IX.F-1). Slurry-phase Fischer-Tropsch synthesis has been investigated in bubble column slurry reactors (IX.F-2, IX.F-3) using promoted, precipitated iron catalysts. These studies have demonstrated that synthesis gas with a H_2/CO ratio of 0.67 can be processed with high conversion at 260 to 270°C and 12 to 15 atm.

Several kinetic studies have been carried out over iron-based catalysts in vapor phase and slurry reactors as evidenced in the literature (IX.F-4 - IX.F-8). Mechanically stirred slurry reactors have been used as these are more suitable to obtain intrinsic kinetic data. Table 1 lists reaction rate expressions commonly utilized.

Table IX.F-1

Proposed Reaction Rate Expressions Proposed in the Literature over Iron-Based Catalysts

Equation	Reaction Rate Expression	Reference No.
(1)	$-r_{CO+H_2}=kP_{CO}P_{H_2}/(P_{CO}+bP_{H_2O})$	1,2
(2)	$-r_{CO+H_2}=kP_{CO}P_{H_2}^2/(P_{CO}P_{H_2}+bP_{H_2O})$	3
(3)	$-r_{CO+H_2}=kP_{CO}P_{H_2}/(P_{CO}+bP_{H_2O})$	4

From the nature of the reaction rate expressions developed, it can be clearly seen that a consensus is lacking for the proper rate equation. Especially important for process

design is the role played by water and/or carbon dioxide in the suppression of the reaction rate at higher synthesis gas conversions.

The kinetic rate equations (1) and (3) might apply to ranges of water-gas shift activity. Equation (1) appears applicable when WGS activity is low ehile (3) is applicable when WGS activity is high, i.e., close to equilibrium.

A high activity precipitated iron-based catalyst has been developed at our laboratory. The kinetics of synthesis gas conversion is investigated over the catalyst in this study. Conversion data have been obtained over the catalyst for a wide range of conversion levels (15-85%) at reaction conditions similar to those in the bubble column studies. The partial pressures and reaction rates of the reaction components have been calculated from the analysis of the reaction products. The results are useful in optimizing the utilization of the catalyst to produce hydrocarbons. Further, a number of possible reaction rate expressions have been tested with the experimental data and an optimum reaction rate expression has been developed for this catalyst.

EXPERIMENTAL

Catalyst

A precipitated iron catalyst containing silica and potassium was prepared by continuous co-precipitation in a polytetrafluoroethylene (PTFE) stirred open tank. Tetraethyl ortho silicate was placed in excess water to form a colloidal suspension and then clear suspension, which was then added to an iron (III) nitrate solution to provide the molar ratio 100 Si/Si + Fe = 4.4. The resulting mixture and concentrated ammonium hydroxide were separately pumped to the precipitation tank at a rate to maintain a pH of about 9 and an average residence time of 6 min. The resulting slurry was continuously withdrawn and filtered using three rotary vacuum drum filters in

parallel. After two washes and re-filtering, the filter cake was dried in an air-flow oven at 100°C. Potassium was added to this catalyst as potassium tertiary butoxide during the loading of the Fischer-Tropsch reactor. The amount of potassium added is such as to obtain a potassium:iron weight ratio of 0.005. The final composition of the catalyst was 61.8 wt. % Fe, 0.897 wt. % Si and 0.311 wt. % K. The BET surface area of the dried catalyst was 284 m^2/g.

Reaction System

A schematic of the reaction system is given in Figure IX.F-1. Carbon monoxide is purified using lead oxide on alumina pellets to remove any carbonyls present. The feed gas (CO and H_2) flow rates are measured and controlled by two separate mass flow controllers (Brooks Instruments Model 5878) before they are mixed in a 0.5 liter vessel and then fed to the reactor. The reactor is a 1-liter stirred autoclave from Pressure Products Industries with a magnetically driven stirrer. The reactant gases are fed below the stirrer blades and the vapor phase products exit at the top of the reactor. A thermocouple and pressure gauge measure the temperature and pressure inside the reactor.

The vapor phase products from the reactor pass through a stainless steel fritted filter into two traps connected in series. The first trap is maintained at 100°C to condense the high boiling products (wax) from the reactor. The second trap is maintained at 0°C which serves to condense the lighter hydrocarbons (oil) and most of the water in the product stream. The uncondensed gases then pass through a Tescom back pressure regulator (used to control the reactor pressure) and a soap bubble flow meter (used to measure the uncondensed gas flow rate). Periodically the composition of the uncondensed gases are measured (see below).

The condensed liquids in the two traps are collected during a mass balance period and separated into a hydrocarbon and aqueous phase. The two phases are analyzed separately to obtain the weight/mole fractions of water, oxygenates and hydrocarbons in the collected liquids.

There is a provision for intermittent sampling of the reactor liquid which passes to a trap maintained at 200°C (Rewax). However, samples of the reactor liquid were not obtained during this study and the heavy hydrocarbons were allowed to accumulate in the reactor during the run.

Product Analysis

The composition of the uncondensed gases from the reactor is obtained using two gas chromatographs designated as GC A and GC B in Figure IX.F-1. GC A is a Carle Gas Analyzer (Hach Series 400 A) which is used to obtain the mole fractions of CO, H_2, CO_2 and C_1 to C_4 paraffins and olefins. GC B is a Hewlett Packard 5790A gas chromatograph with a Porapak Q column and a thermal conductivity detector. GC B is used to obtain the mole fractions of water and C_4 to about C_9-C_{10} hydrocarbons in the uncondensed product stream.

The aqueous phase of the condensed liquid products is analyzed using GC B to obtain the mole fractions of water and oxygenates. Samples of the hydrocarbon phases from the oil and wax traps are combined (in the same weight ratio as collected) and diluted with an equal weight of carbon disulfide. The composition of this sample is obtained using a Hewlett Packard 5890 Series II gas chromatograph with a DB-5 capillary column and a flame ionization detector.

Procedure

The iron catalyst (5.09) containing silicon is loaded in the reactor which already contains 290 g of melted C_{28} paraffin (at 90°C) and 0.0159 g of potassium is added in the form of potassium tertiary-butoxide. The reactor pressure is built up to 175 psig (1308 kPa) under CO atmosphere with stirring (750 rpm) and the reactor is subsequently heated to 270°C (reaction temperature) at a rate of 2°C/min. Pretreatment of the catalyst is carried out at 270°C, 175 psig (1308 kPa) using CO at a flow rate of 13.345 NL/hr for 24 hours.

At the end of the pretreatment period, synthesis gas flow is started at a H_2/CO ratio of 0.67. During the entire run the temperature in the reactor is 270°C, the pressure is 175 psig (1308 kPa) and the stirring speed is maintained at 750 rpm. About two days are required before the catalyst reaches steady state as evidenced by the constant conversion of synthesis gas. Subsequently, the space velocity of the synthesis gas is varied between 5 and 70 NL/hr/gFe. The conversions of CO, H_2, and the formation of various products are measured with a period of approximately 24 hours at each space velocity. The H_2/CO ratio of the feed synthesis gas is kept constant at 0.67 at all the space velocities. Periodically during the run, the catalyst activity is measured at pre-set "standard" conditions to check for catalyst deactivation.

Data Analysis

The Fischer-Tropsch synthesis can be considered as

$$CO + (1+(m/2))\ H_2 \rightarrow CH_m + H_2O \quad (4)$$

Along with the Fischer-Tropsch reaction, the water gas shift reaction plays a prominent role over iron-based catalysts

$$CO + H_2O \rightarrow CO_2 + H_2 \quad (5)$$

Thus the source of carbon in the Fischer-Tropsch synthesis (carbon monoxide) can be converted to hydrocarbons (desired product) or to carbon dioxide (undesirable product). Other side reactions include the formation of alcohols and the Boudouard reaction. However, they occur to a very limited extent and are not considered in the kinetic analysis.

The conversions of CO, H_2 and synthesis gas are calculated from the inlet and outlet flow rates of these components from the reactor. Since the reactor used is equivalent to a continuous-flow stirred tank reactor (CSTR), the reaction rates as well as the partial pressures of the reaction components are uniform throughout the reactor. Hence the rates of disappearance of CO and H_2 and the rates of formation of products are obtained directly from the observed input and output flow rates. However, there are limitations to obtaining the rates of all the products directly. For instance, the rate of formation of hydrocarbons is difficult to measure accurately as the high molecular weight hydrocarbons do not exit the reactor in the vapor phase but remain in the reactor liquid. The reaction rates are most accurately measured for the reaction components which are predominantly in the vapor phase in the reactor, i.e., CO, H_2, CO+H_2, CO_2 and H_2O. From these directly measured compositions, the rate of the Fischer-Tropsch and the water gas shift reaction can be calculated as

$$r_{FT} = (-r_{CO}) - r_{CO_2} \quad (6)$$

$$r_{WGS} = r_{CO_2} \quad (7)$$

The rate of the Fischer-Tropsch reaction can also be calculated as (8),

$$r_{FT} = r_{CO+H_2}/(2 + (m/2)) \quad (8)$$

This requires an accurate estimation of the H/C ratio of the hydrocarbon products. In general, the H/C ratio varies with carbon number and is difficult to measure accurately as the heavier hydrocarbons are retained in the reactor.

The partial pressures of the reaction components are calculated from the mole fractions of the various products in the vapor stream exiting the reactor. This requires that the composition of the condensed hydrocarbons be determined. The retention of heavy hydrocarbons in the reactor does not pose a problem as these are typically in the liquid phase in the reactor and do not contribute to partial pressures. Further, the amount of initial start up solvent in the condensed hydrocarbon products must also be included in the mole fraction calculations as it could contribute to a substantial partial pressure under certain reaction conditions. The composition of the product liquids is measured and averaged over the total mass balance period to obtain the moles per hour of the liquid products so as to compare the results with the composition of the uncoridensed gas from the on-line gas chromatographs and thus obtain the mole fractions of each product and unconverted reactant in the vapor phase in the reactor.

RESULTS

A reaction run lasted for approximately 12 days. The catalyst activity at pre-set standard conditions during this run (Figure IX.F-2) show that the catalyst activity remained practically constant during the course of the reaction run. The data in Figure IX.F-2 also indicates that the experimental error in the measurement of percentage conversion is about 2%. Material balances at all the space velocities were between 95 to 102%.

The conversions of CO, H_2 and conversion of synthesis gas with space time in the reactor are shown in Figure IX.F-3. The experimental data cover a large range of conversions: for CO the conversions range from 10 to 85%. The change in conversion is much faster at low space times than it is at higher space times. This is similar to observed conversions over a fused iron-based catalyst (IX.F-6). Further at low space times the conversion of H_2 is greater than the conversion of CO while at higher space times the situation is reversed. The synthesis gas conversion at which the conversions of both CO and H_2 become equal is about 70%. Obviously the water gas shift reaction plays a role in the relative conversions of CO and H_2. This is referred to later in the discussion section.

Figure IX.F-4 shows the calculated partial pressures of the various components in the vapor phase in the reactor as a function of space time. As expected, the partial pressures of CO and H_2 decrease with space time while the partial pressures of CO_2 and hydrocarbons increase with space time. The partial pressure of water initially increases with space time and then decreases indicating that it is an intermediate. This is also as expected since the water gas shift reaction consumes water formed

from the Fischer-Tropsch synthesis. Of particular interest is the low partial pressure of water as compared to the other reaction components over the large range of conversions studied, and especially the attainment of the highest partial pressure at a low CO conversion. Further, the variation in water partial pressure is small (between 4 to 11 psia) as compared to the variation in partial pressures of the other reaction products. This implies that the catalyst used is a good water gas shift catalyst and converts the greater amounts of water formed by the Fisher-Tropsch reaction at high synthesis gas conversions.

Figure IX.F-5 shows the calculated rates of disappearance of CO, H_2, synthesis gas and the rates of formation of water and CO_2 with space time. The rate of disappearance of H_2 decreases with space time as does the rate of formation of water. The rate of disappearance of synthesis gas is approximately constant at small space times and then decreases monotonically with increasing space time. Both the rate of disappearance of CO and the rate of formation of CO_2 pass through a maximum with increasing space time.

Figure IX.F-6 shows the reaction quotient (RQ) of the water gas shift reaction:

$$RQ = P_{CO_2} P_{H_2} / P_{CO} P_{H_2O} \qquad (9)$$

as a function of space time. The value of the equilibrium constant of the water gas shift reaction at 270°C is 62. As shown in Figure IX.F-6, the water gas shift reaction is not at equilibrium at any of the space velocities studied. Further, the highest value of the reaction quotient, or the extent of approach of the water gas shift to equilibrium, is 18 as compared to the equilibrium value of 62. This indicates that the rate of the

backward reaction is much less than the rate of the forward reaction over the catalyst studied.

Examples of the hydrocarbon selectivity plots obtained are shown in Figure IX.F-7. These plots were obtained at low, intermediate and high conversions. The plots at intermediate and high conversions indicate that the selectivity can be characterized by a single value of the hydrocarbon chain growth probability, α, of about 0.74. However, the plot at low conversion shows a pronounced hump at intermediate carbon numbers. Note that the order in which the data is obtained is intermediate conversion first, then low conversion and finally high conversion. Thus the hump exhibited by the selectivity plot at low conversions is perhaps due to the "flashing off" of intermediate carbon number hydrocarbons (C_{15} to C_{30}) previously accumulated in the reactor liquid. Such a flashing off is to be expected due to the high gas flow rates at the low conversions. Further, the amount of the start-up solvent, C_{28} paraffin, is also much higher in the condensed hydrocarbon products at low conversions (about 10-20 wt.%) than at intermediate and high conversions (about 3-5 wt.%). This is consistent with the hypothesis of intermediate range hydrocarbons flashing off at low conversions.

Figure IX.F-8 shows the selectivity to alkanes exhibited by the C_2 and C_3 hydrocarbons as a function of space time. The selectivity to alkanes for both hydrocarbons increases with space time. Thus the hydrocarbon products at low conversions are more olefinic while at high conversions they are more paraffinic. This is also indicated by the average H/C ratio of the hydrocarbon products with space time (Figure IX.F-9). As the space time or conversion increases, the H/C ratio initially

remains constant and then increases indicating a more paraffinic product at high space times.

The selectivity towards alkanes as a function of carbon number at low, intermediate and high conversions (Figure IX.F-10) are quite similar at each of these conversions. All the plots exhibit a minimum alkane selectivity at C_3 or C_5 hydrocarbons. The value of the alkane selectivity at high carbon numbers (above 20-25) is one indicating that these hydrocarbons are completely paraffinic.

The reaction rates for formation of products and the disappearance of reactants are used to calculate the rate of the Fischer-Tropsch reaction and the rate of the water gas shift reaction from Equations (6), (7) and (8). These rates are plotted as a function of space time (Figure IX.F-11) and show that the rate of the Fischer-Tropsch reaction is always greater than the rate of the water gas shift reaction. However, at high conversions of synthesis gas (above about 55%) the rate of the water gas shift reaction closely approaches the rate of the Fischer-Tropsch reaction. The rate of the Fischer-Tropsch reaction has been calculated by two methods: from the observed CO and CO_2 rates (Equation (6)) and from the observed H/C ratio of the hydrocarbon products (Equation (8)). The two methods give approximately the same values of the Fischer-Tropsch reaction rates (within 10%) as shown in the parity plot in Figure IX.F-12. Up to about 40% conversion, the rate of the Fischer-Tropsch reaction is approximately constant after which it monotonically decreases. In contrast, the rate of the water gas shift reaction passes through a maximum with increasing synthesis gas conversion.

DISCUSSION

It is of interest to note the relative conversions of CO and H_2 as the space time in the reactor is increased. The conversion of H_2 is greater than the conversion of CO at low space times while the reverse is true at higher space times. The exit H_2/CO ratio initially decreases and then increases as the conversion of CO increases (Figure IX.F-13). At 70% CO conversion, the exit H_2/CO ratio is the same as the inlet H_2/CO ratio. This is a result of the two competing reactions taking place in the reactor: Fischer-Tropsch and the water gas shift.

If we take as the basis 1 mole of CO entering the reactor along with 0.67 moles of H_2 and if x moles of CO react to form hydrocarbons (Fischer-Tropsch) while z is the total moles of CO reacted, then Equations (4) and (5) can be written as

$$xCO + x(1+m/2)H_2 \rightarrow xCH_m + xH_2O \tag{10}$$

$$(z-x)\ CO + (z-x)\ H_2O \rightarrow (z-x)\ CO_2 + (z-x)\ H_2 \tag{11}$$

Since H_2O must be formed from the Fischer-Tropsch reaction to react in the water gas shift reaction,

$$x \geq z-x \tag{12}$$

$$i.e.,\ x/z \geq 0.5 \tag{13}$$

It can be shown that

$$\text{If } X_{H_2}/H_{CO} \begin{matrix} > 1 \\ = 1 \\ < 1 \end{matrix} \text{ then } (x/z) \begin{matrix} > \\ = \\ < \end{matrix} 5/3(2+m/2) \tag{14}$$

Similarly

$$\text{If exit } H_2/CO \begin{matrix} > 1 \\ = 1 \\ < 1 \end{matrix} \text{ then } (x/z) \begin{matrix} > \\ = \\ < \end{matrix} 5/3(2+m/2) \qquad (15)$$

Thus the relative values of both the conversions of H_2 to CO and the exit H_2/CO ratio are dependent on (x/z); i.e., the fraction of CO converted which forms hydrocarbons. This is plotted in Figure IX.F-14 as a function of CO conversion. Up to a CO conversion of 70%, the conversion of H_2 is greater than the conversion of CO and hence the fraction of CO converted producing hydrocarbons (x/z) is greater than 5/3(2+m/2). The fraction of CO converted producing hydrocarbons (x/z) decreases as CO conversion increases and approaches the value of 5/3(2+m/2) at 70% CO conversion where the conversion of H_2 and CO are equal. At 70% CO conversion the value of x/z is about 0.53 (Figure IX.F-14). Note that the value of x/z cannot be less than 0.5 according to Equation (13). Hence, above 70% CO conversion, the change in x/z should be much less than that below 70% CO conversion; in fact, it appears that x/z remains approximately constant instead of decreasing further (Figure IX.F-14). This is a consequence of the concurrent increase in the value of m, the H/C ratio of the hydrocarbon products, as shown in Figure IX.F-9.

An important conclusion to be drawn from this is that it would be more desirable to limit the Fischer-Tropsch synthesis from low to intermediate conversion levels. At intermediate conversions the fraction of CO being converted to the undesirable product CO_2 is lower and, correspondingly, the fraction of CO converted producing the desired product hydrocarbons is higher. Higher overall conversions can be achieved by either having two reactors in series or a single reactor with recycle.

The exit H_2/CO ratio, which is also the H_2/CO ratio in the reactor, plays an important role in the increased selectivity towards paraffins that this catalyst displays at high space times/conversions. A plot of the average H/C ratio of the hydrocarbon products versus the H_2/CO ratio (Figure IX.F-15) indicates that a linear relationship exists between these variables. This is expected as a higher H_2/CO ratio would lead to a higher amount of saturated hydrocarbon. Thus the selectivity towards paraffins, and the H/C ratio of the hydrocarbon products, should increase with the H_2/CO ratio.

The experimental data obtained in this study also allow a test for the various reaction rate expressions proposed in the literature for Fischer-Tropsch synthesis over iron-based catalysts. For the purpose of testing these rate expressions against the experimental data, they are rearranged so as to obtain a linear relationship. The experimental data are then plotted according to this linear relationship to determine if a straight line gives a good fit to the data obtained. The rearranged reaction rate expressions from those given in Table1 are given below:

$$P_{H_2}/-r_{CO+H_2} = (1/k) + (b/k)\ (P_{H_2O}/P_{CO}) \tag{16}$$

$$P_{H_2}/-r_{CO+H_2} = (1/k) + (b/k)\ (P_{H_2O}/P_{CO}P_{H_2}) \tag{17}$$

$$P_{H_2}/-r_{CO+H_2} = (1/k) + (b/k)\ (P_{CO_2}/P_{CO}) \tag{18}$$

As shown in Figures IX.F-16, IX.F-17 and IX.F-18, none of the three expressions in the literature are able to give a good fit to the data obtained in this study. However, a reaction rate expression which represents the experimental data well is given below:

Rearranging this expression, we get,

$$-r_{CO+H_2} = k\, P_{CO} P_{H_2} / (1 + K_{CO} P_{CO}) \quad (19)$$

$$P_{CO} P_{H_2} / -r_{CO+H_2} = (1/k) + (K_{CO}/k)\, P_{CO} \quad (20)$$

A reasonably good fit is obtained of the experimental data to the rearranged rate expression (Figure IX.F-19). The value of the rate constant, k, calculated from the intercept is 2.43×10^{-5} moles/hr-gFe-kPa^2. The value of the adsorption equilibrium constant for CO calculated from both the slope and the intercept is 2×10^{-2} kPa^{-1}.

This rate expression differs from the proposed rate expressions in Table IX.F-1 since there is no (or negligible) inhibition of the rate by the reaction products (water and/or CO_2) and no (or negligible) competition between the adsorption of CO and the reaction products (water and/or CO_2). A possible reason for this difference in the case of one of the reaction products, water, is the low and almost constant partial pressure of water obtained at all the space velocities studied. Hence any effect of water on the reaction rate would appear to be low. However, this explanation does not hold for the other reaction product, namely carbon dioxide. The partial pressure of CO_2 varies considerably with space velocity. Hence it can be concluded that CO_2 does not influence the reaction rate over the catalyst used in this study.

A thorough study of the kinetics of the Fischer-Tropsch reaction (IX.F-10) at various temperatures (with the C-73 catalyst) showed that the reaction rate expression, equation (2) in Table IX.F-1, was able to represent the experimental data well at 232 and 248°C whereas at a higher temperature of 262°C the data were better fit with the reaction rate expression given in Equation (19). An explanation given was that this is due to the adsorption equilibrium constant for water becoming low at high

temperatures contributing to the negligible effect of water on the reaction rate. This provides another explanation for the difference between the reaction rate expression developed in this study as compared to previous investigations as the reaction temperature in this study is higher than 262°C (270°C).

The rate of synthesis gas conversion is a resultant of the Fischer-Tropsch and water gas shift reactions. Since the rates of these individual reactions can be calculated their kinetics can also be studied. Figure IX.F-19 shows a plot for the kinetics of the Fischer-Tropsch reaction according to the linearized version of the rate expression given in Equation (19). The rate of the Fischer-Tropsch reaction calculated by both methods (Equations (6) and (8)) are shown. Figure IX.F-20 indicates that the Fischer-Tropsch reaction can be adequately represented by the rate equation:

$$r_{FT} = K_{FT}P_{CO}P_{H_2}/(1+K_{CO}P_{CO}) \qquad (21)$$

which is similar to the rate expression for the synthesis gas conversion. The value of the rate constant, k_{FT}, is 6.08×10^{-6} moles/hr-gFe-kPa^2 while the value of the adsorption equilibrium constant for CO, K_{CO}, is 1.7×10^{-2} kPa^{-1}. The value of K_{CO} is in close agreement with that determined for the synthesis gas conversion.

Earlier studies (IX.F-3, IX.F-8) considered the rate expression for the water gas shift reaction as a mass action rate divided by the same denominator as for the synthesis gas conversion. With respect to the rate expression developed for the synthesis gas conversion in this study the rate of the water gas shift reaction should then be given as:

$$r_{WGS} = k_{WGS}(P_{CO}P_{H_2O} - (P_{CO_2}P_{H_2}/K_{eq}))/(1 + K_{CO}P_{CO}) \quad (22)$$

A linearized version of this rate expression suitable for testing against the experimental data is:

$$(P_{CO}P_{H_2O} - (P_{CO_2}P_{H_2}/K_{eq}))/r_{WGS} = (1/k_{WGS}) + (K_{CO}/k_{WGS})P_{CO} \quad (23)$$

Figure IX.F-21 shows a plot to test this reaction rate expression against the experimental data obtained in this study. A good linear fit is obtained but the intercept of the best fit straight line is negative, indicating a negative value for the rate constant of the water gas shift which is obviously not possible. To develop an alternative rate expression one must consider the low partial pressure of water at all the space velocities used in this study. Thus, the data in Figure IX.F-4 indicate that the partial pressure of water is always much less than the partial pressure of CO and that water is therefore the limiting reactant for the shift reaction. Hence it is more appropriate that the rate expression for the shift reaction would be dependent on the partial pressure of water and be largely independent of the CO partial pressure. Considering further that the shift reaction is far from equilibrium, as shown by the values of the reaction quotient (RQ), the rate expression for the water gas shift can be written as

$$r_{WGS} = k_{WGS}P_{H_2O} \quad (24)$$

The experimental data appear to fit a variant of this rate expression well for a value of the exponent for the water partial pressure of 0.68. The best fit rate expression for the shift reaction as shown in Figure IX.F-22 is then given as:

$$r_{WGS} = k_{WGS} P_{H_2O}^{0.68} \quad (25)$$

This indicates that the shift reaction is perhaps weakly inhibited by the partial pressure of water.

CONCLUSIONS

The Fischer-Tropsch synthesis has been studied over an iron based catalyst containing silica and potassium in a mechanically stirred slurry reactor. A wide range of synthesis gas conversions were obtained by varying the space velocity. Partial pressures and reaction rates of reaction components were determined at each conversion.

The experimental results show that: (i) the rate of the water gas shift reaction is lower than the rate of the Fischer-Tropsch reaction at lower conversions (< 60%) whereas it closely approaches the rate of the Fischer-Tropsch synthesis at high conversions, (ii) the fraction of CO converted to hydrocarbons is higher at low and intermediate conversions whereas it is smaller at high conversions. These findings suggest that it would be beneficial to carry out the reaction at intermediate conversions. This would result in an optimum use of CO to produce hydrocarbons rather than CO_2. High overall conversions can be obtained by either using a second reactor or recycling the product gas using a single reactor.

The hydrocarbon products are characterized by a single chain growth probability, α, of about 0.74. The hydrocarbon products are more paraffinic at high space times/conversions than at low space times/conversions. This is related to the H_2/CO ratio in the reactor which increases at high space times/conversions.

The reaction rate expression for synthesis gas conversion developed for this catalyst is:

$$-r_{CO+H_2} = k\, P_{CO} P_{H_2} / (1 + K_{CO} P_{CO})$$

The rate expression shows that CO is strongly adsorbed on the catalyst and that the reaction products such as water and CO_2 do not (or negligibly) inhibit the reaction rate. A similar reaction rate expression also holds for the Fischer-Tropsch reaction. The water gas shift reaction is a function of the partial pressure of water alone.

Finally, the partial pressure of water attains a maximum value at low conversion levels (40% or less) and slowly declines for higher CO conversion levels.

ACKNOWLEDGMENT

This work was supported by U.S. DOE contract number DE-AC22-94PC94055 and the Commonwealth of Kentucky.

REFERENCES

IX.F-1. V.U.S. Rao, G.J. Stiegel, G.J. Cinquegrane and R. D. Srivastava, *Fuel Proc. Technol.* , **30**, (1992) 83.

IX.F-2. H. Kölbel and M. Ralek, *Catal. Rev. -Sci. Eng.* , **21**, (1980) 225.

IX.F-3. J. C. W. Kuo, Final Report DOE Contract No. DE-AC22-80PC30022, Mobil Research and Development Corp., Paulsboro, NJ (1983).

IX.F-4. R. B. Anderson, in "Catalysis", Vol. IV, Emmett, P. H., (Editor), Rheinhold, New York (1956).

IX.F-5. H. E. Atwood and C. O. Bennett, *I&EC Proc. Des. Dev.* , **18**, (1979) 163.

IX.F-6. G. A. Huff and C. N. Satterfield, *I&EC Proc. Des. Dev.* , **23**, (1984) 696.

IX.F-7. S. H. Ledakowicz, H. Nettlehoff, R. Kokuun and W-D. Deckwer, *I&EC Proc. Des. Dev.* , **24**, (1985) 1043.

IX.F-8. W. H. Zimmerman and D. B. Bukur, *Canadian J. Chem. Eng.* , **68**, (1990) 292.

IX.F-9. D. S. Newsome, *Catal. Rev. - Sci. Eng.*, **21**, (1980) 275.

IX.F-10. G. A. Huff, Sc. D. Thesis, M. I. T. Cambridge, Mass. (1982).

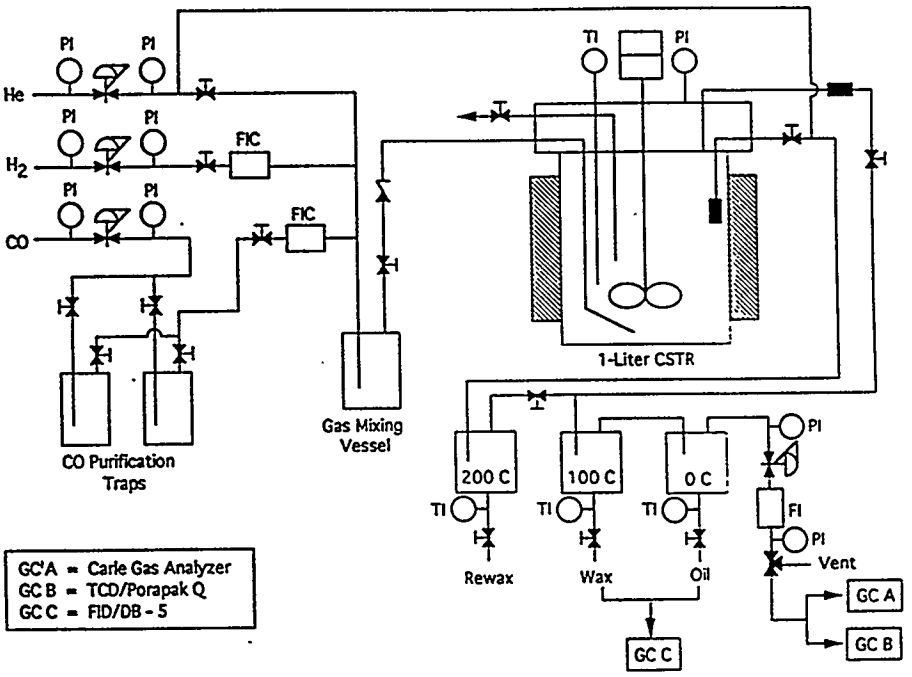

Figure IX.F-1. Schematic of Fischer-Tropsch reactor system.

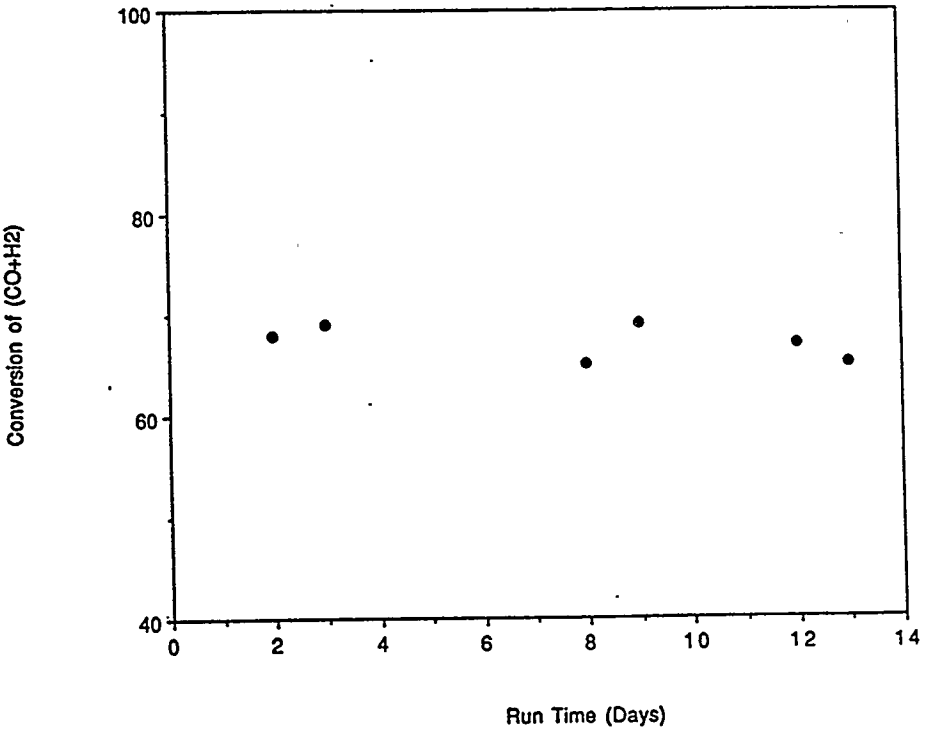

Figure IX.F-2. Synthesis gas conversion at "standard conditions" during experimental run.

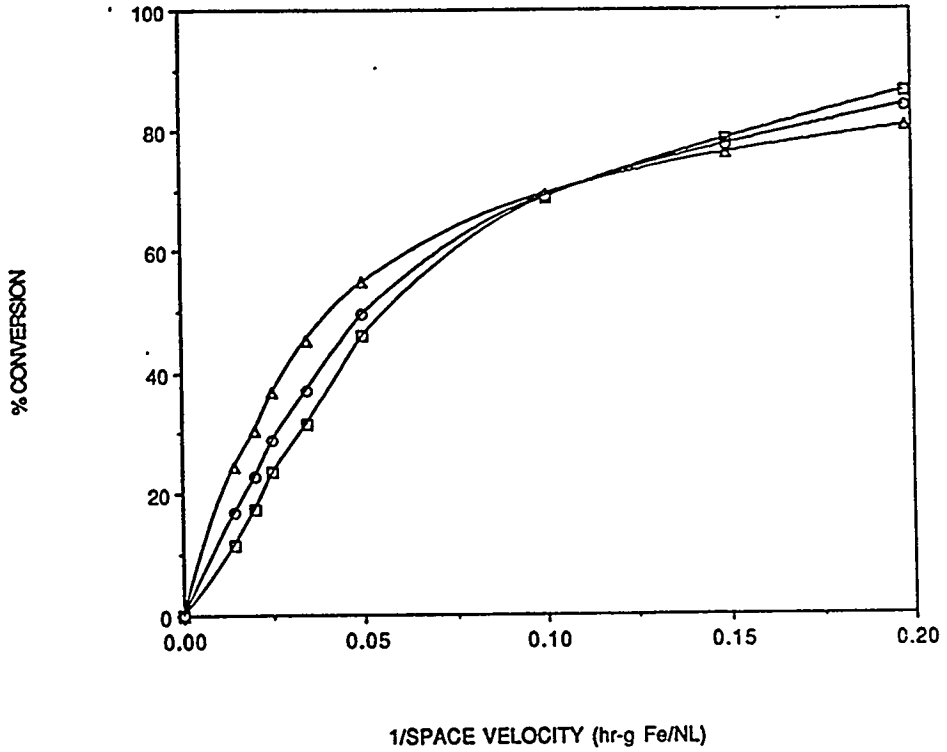

Figure IX.F-3. Conversions of CO (□), H_2 (△) and synthesis gas (○) as a function of the inverse of space velocity.

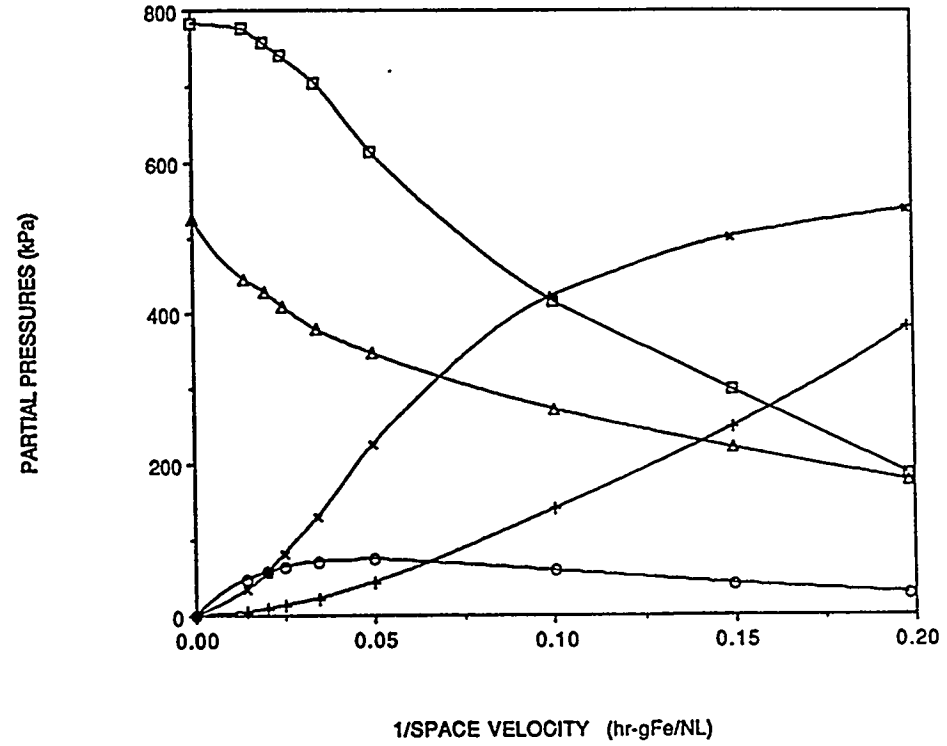

Figure IX.F-4. Partial Pressures of CO (□), H_2 (△), CO_2 (X), H_2O (○) and hydrocarbons (+) as a function of the inverse of space velocity.

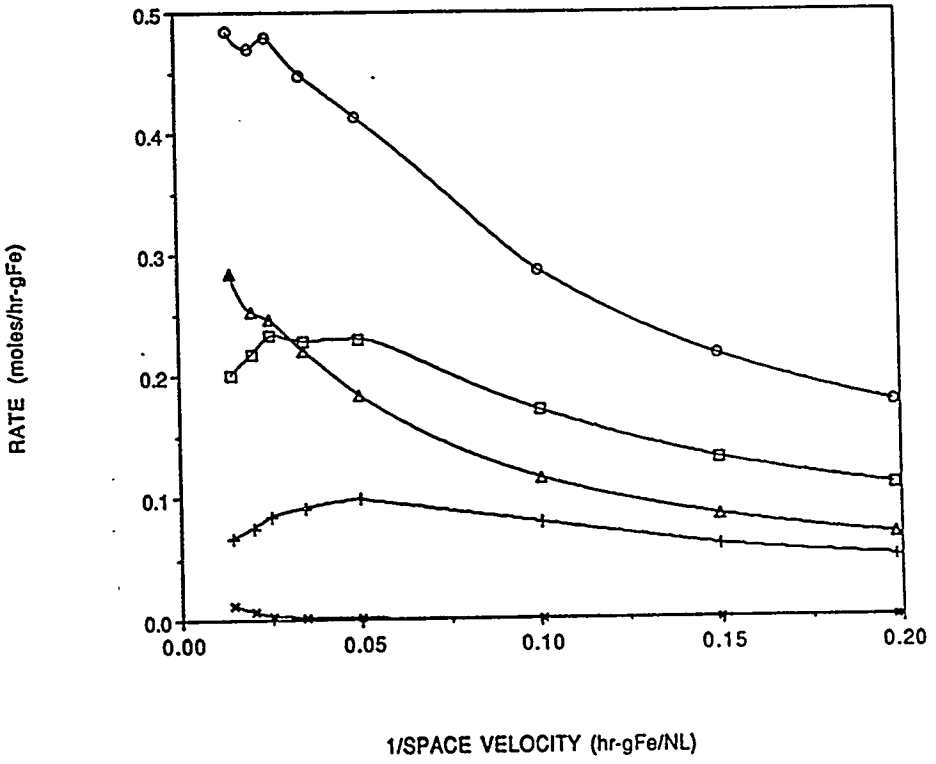

Figure IX.F-5. Rates of disappearance of CO (□), H_2 (△), synthesis gas (○) and rates of formation of CO_2 (+) and H_2O (X) as a function of the inverse of space velocity.

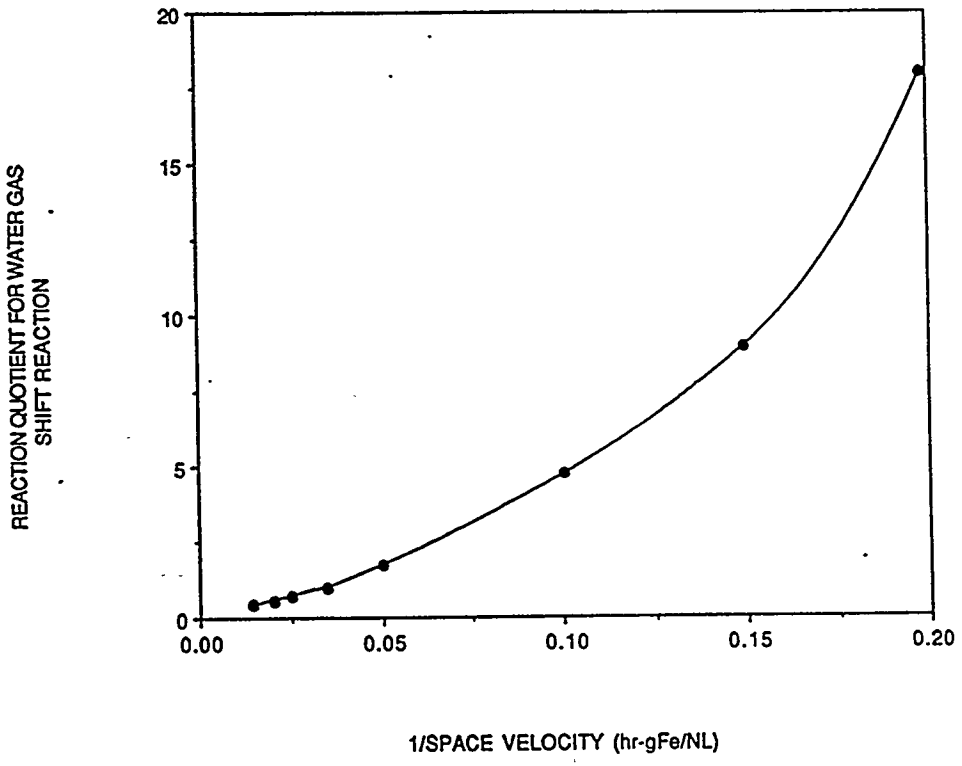

Figure IX.F-6. Reaction quotient of the water gas shift reaction as a function of the inverse of space velocity.

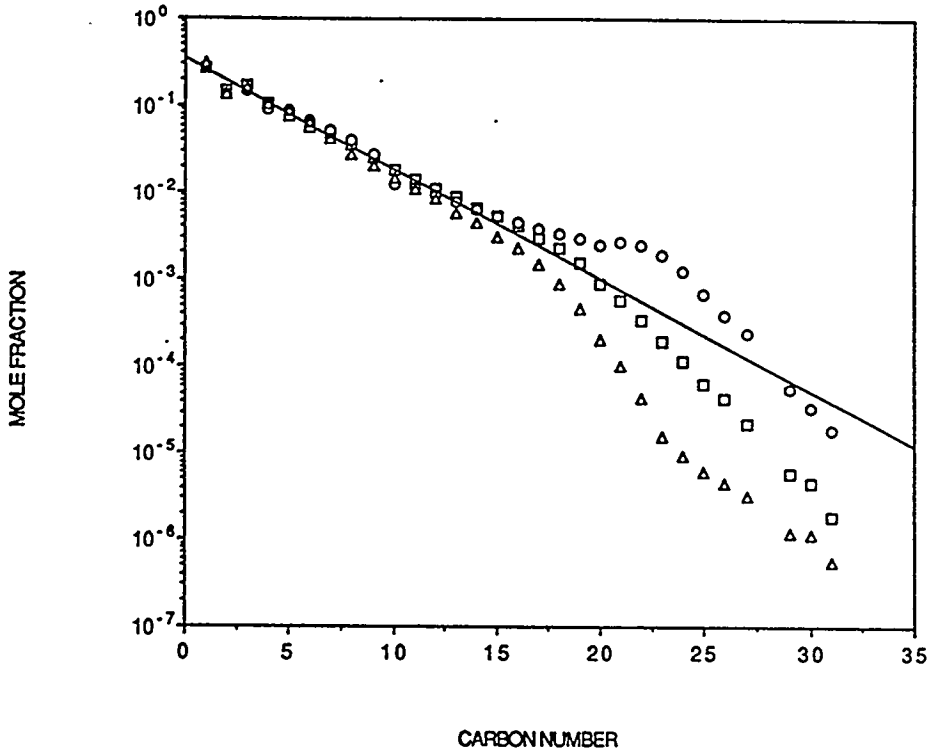

Figure IX.F-7. Examples of hydrocarbon selectivity plots at synthesis gas conversions of 22% (○), 49% (□) and 85% (△).

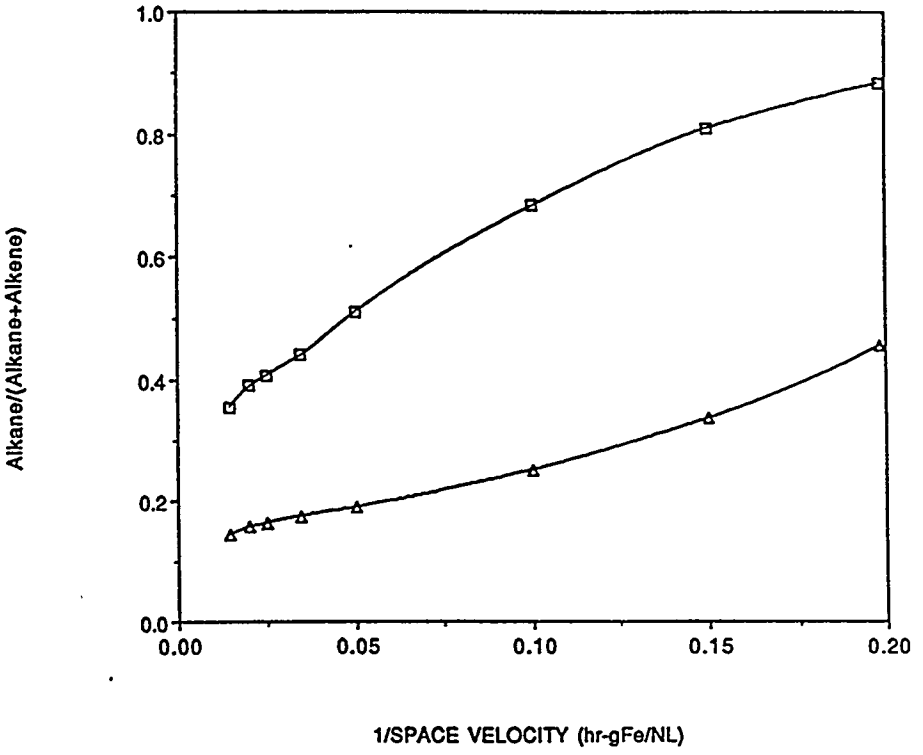

Figure IX.F-8. Selectivity to alkanes for C_2 (□) and C_3 (△) as a function of the inverse of space velocity.

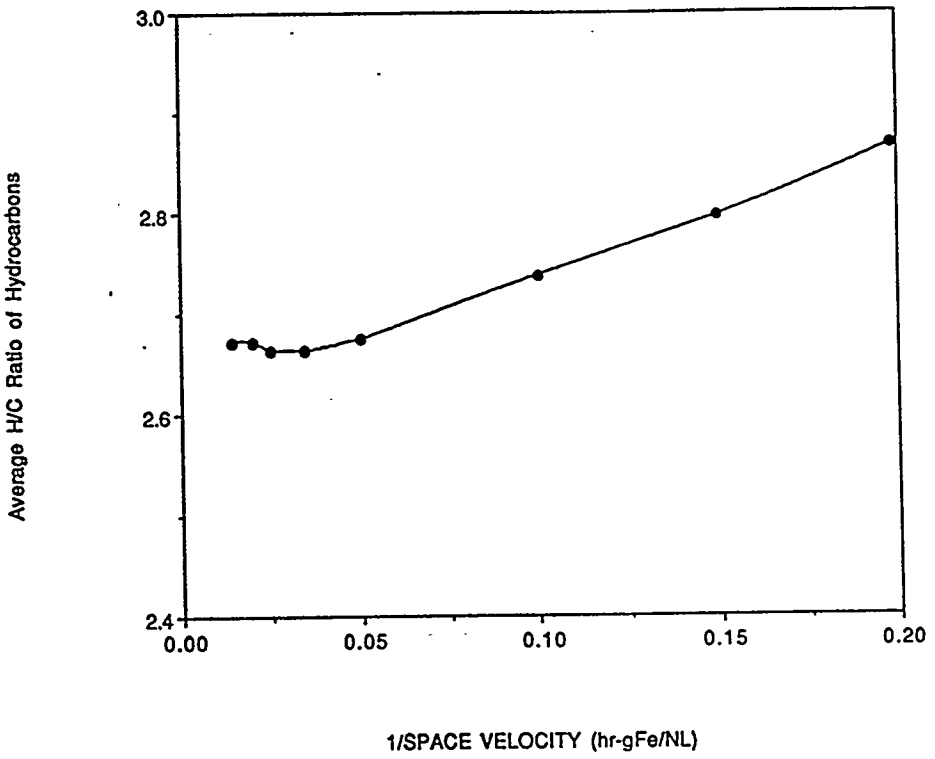

Figure IX.F-9. Average H/C ratio of hydrocarbon products as a function of the inverse of space velocity.

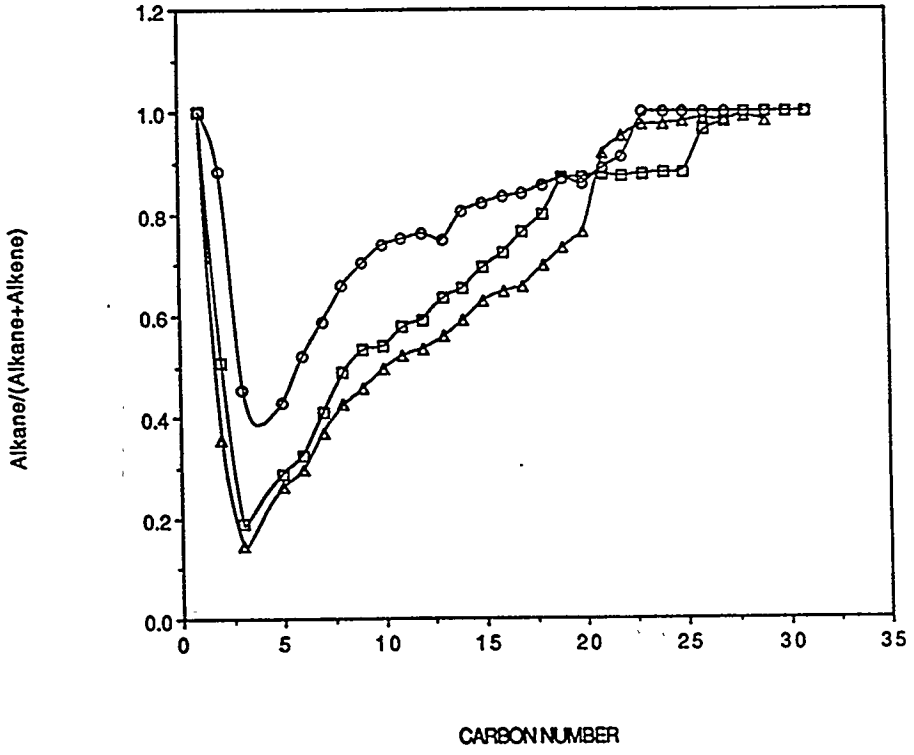

Figure IX.F-10. Selectivity to alkanes as a function of carbon number at synthesis gas conversions of 16% (△), 49% (□) and 85% (○).

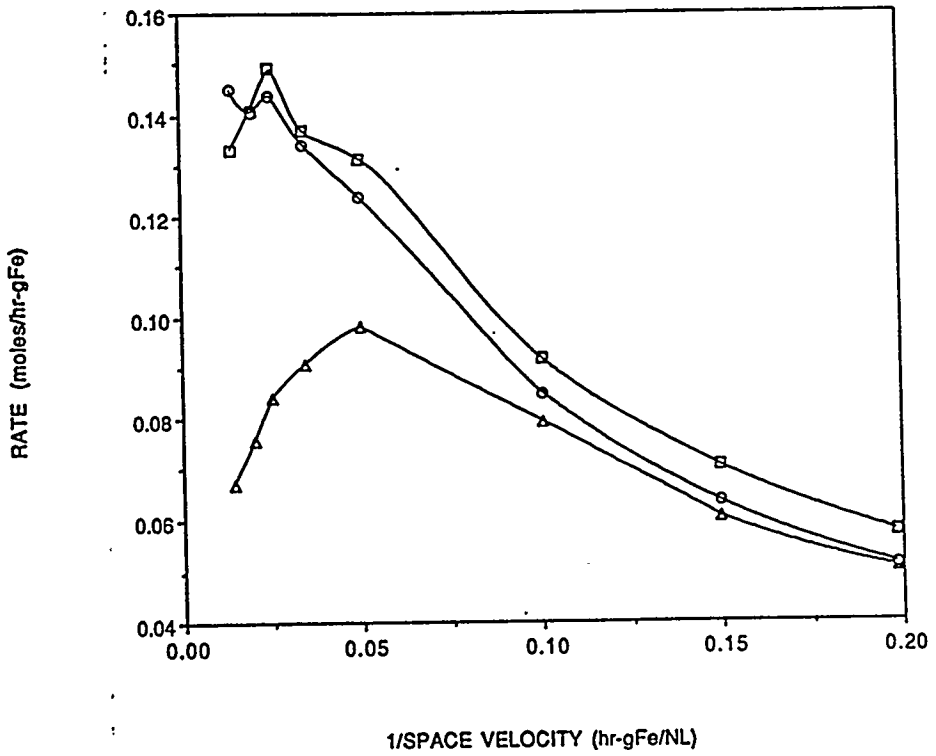

Figure IX.F-11. Rates of the Fischer-Tropsch reaction calculated from Equation (6) (□) and Equation (8) (○) and the water gas shift reaction (△).

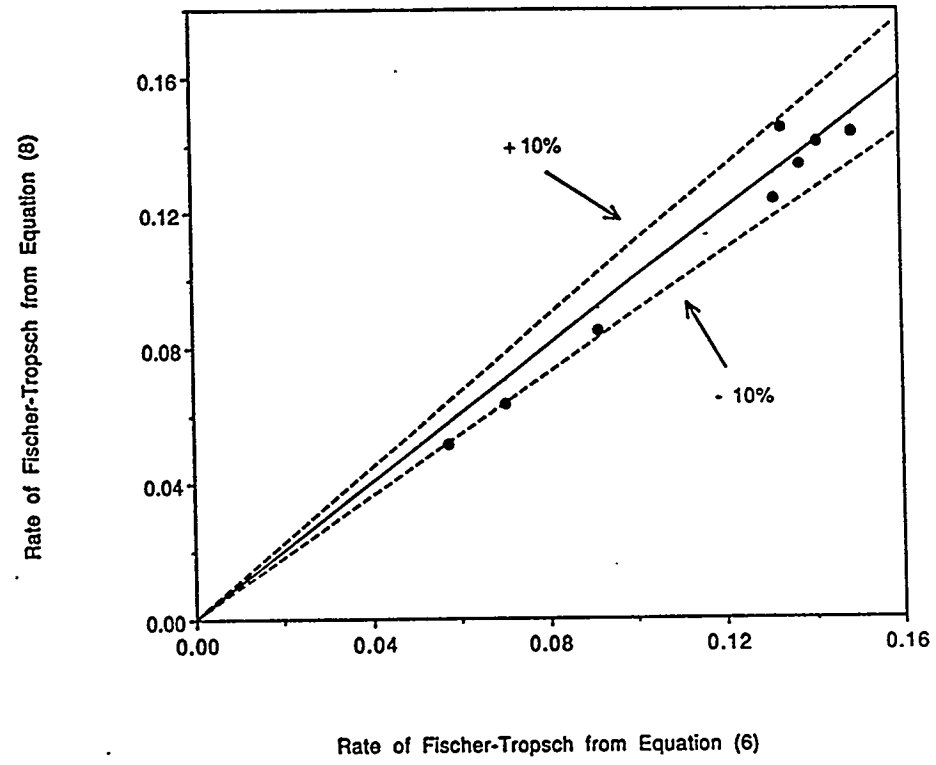

Figure IX.F-12. Parity plot of the Fischer-Tropsch reaction rate as calculated from Equations (6) and (8).

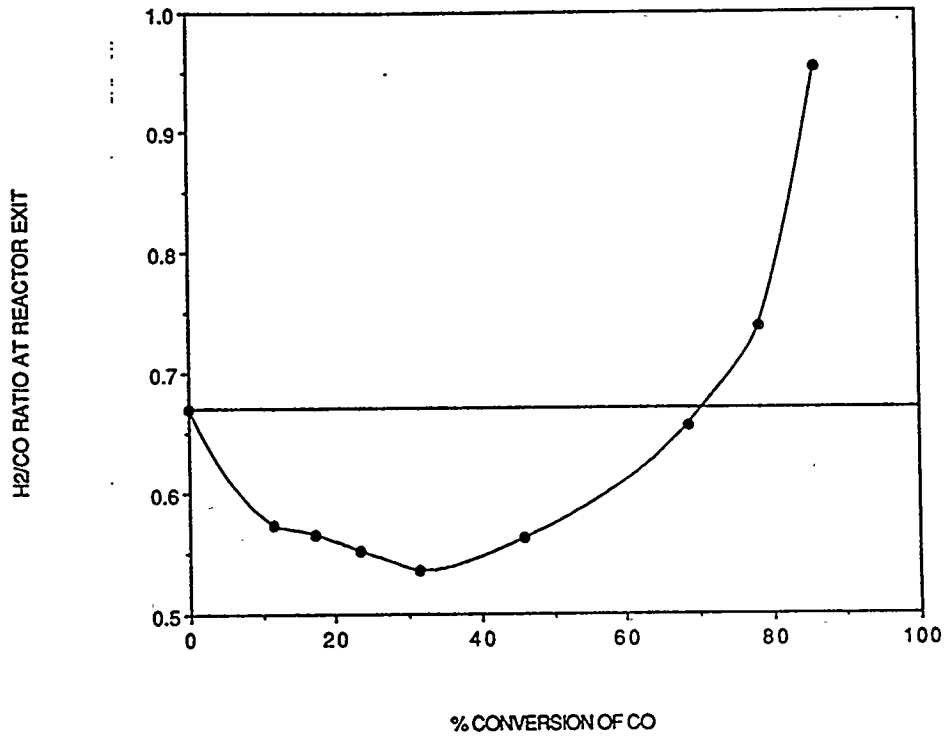

Figure IX.F-13. Exit H_2/CO ratio as a function of CO conversion.

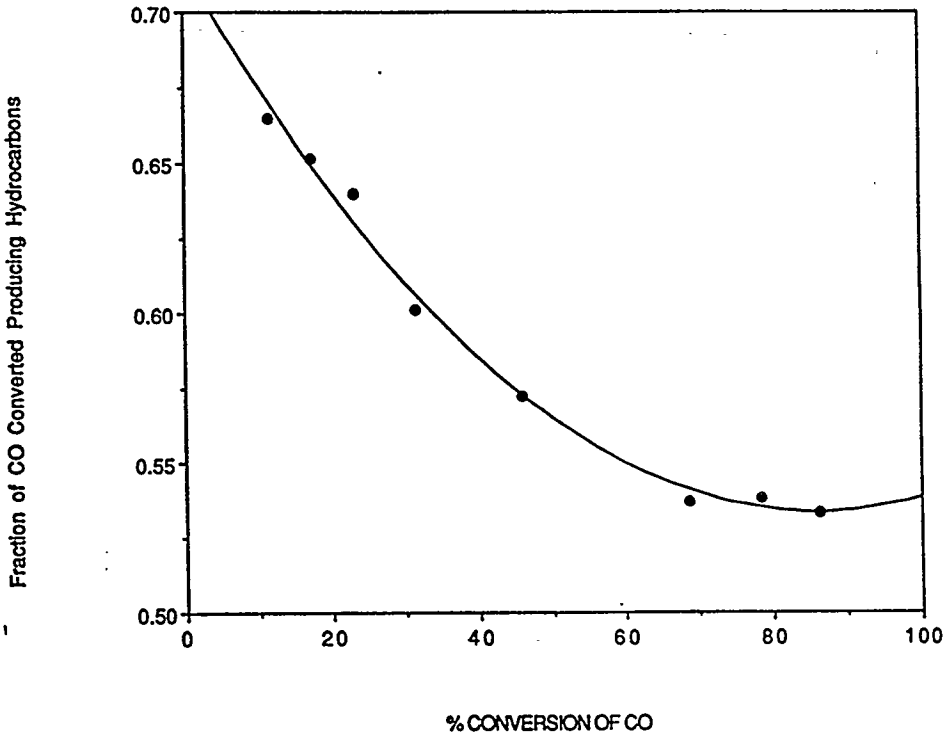

Figure IX.F-14. Fraction of CO converted producing hydrocarbons as a function of CO conversion.

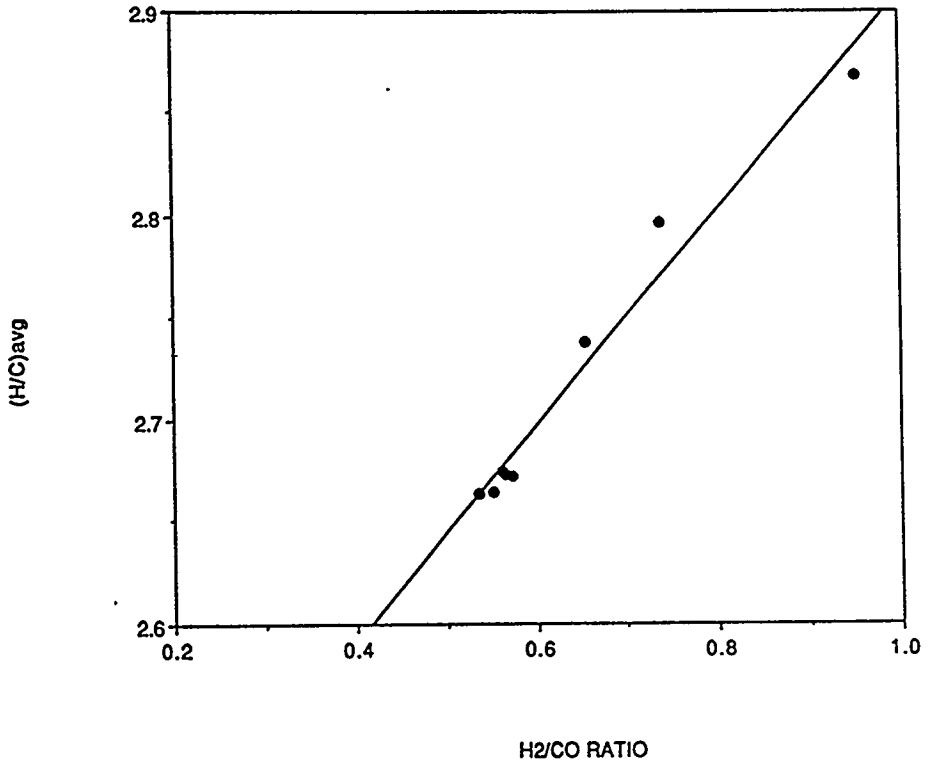

Figure IX.F-15. Average H/C ratio of hydrocarbon products as a function of the exit H_2/CO ratio.

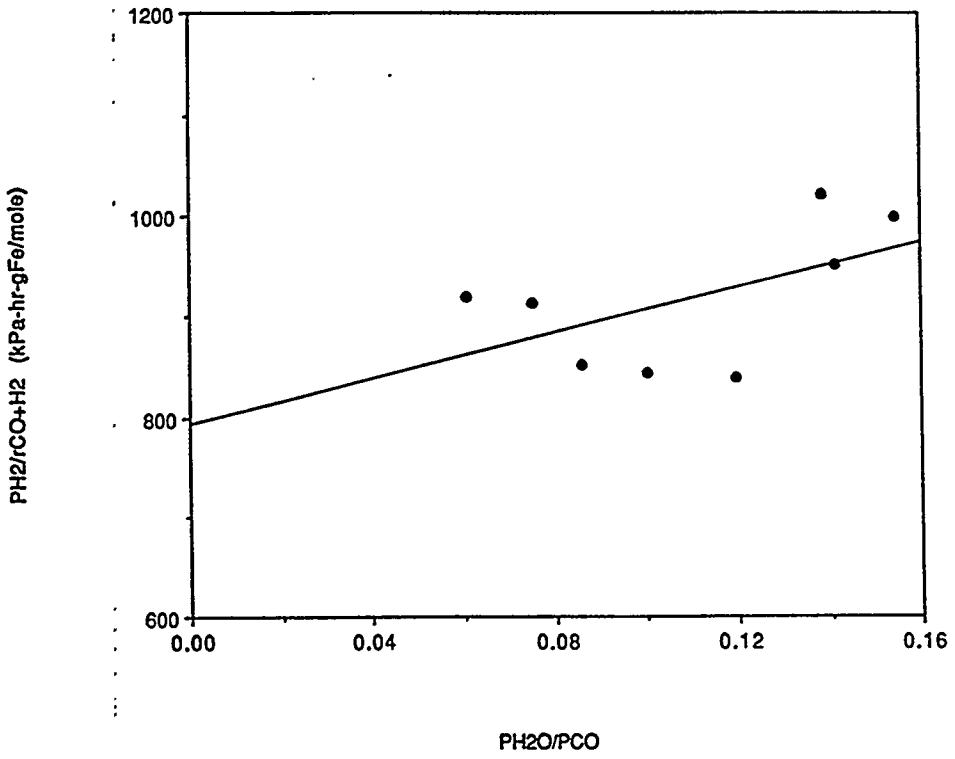

Figure IX.F-16. Test for reaction rate expression (Equation (1)) given in its linearized form by Equation (16).

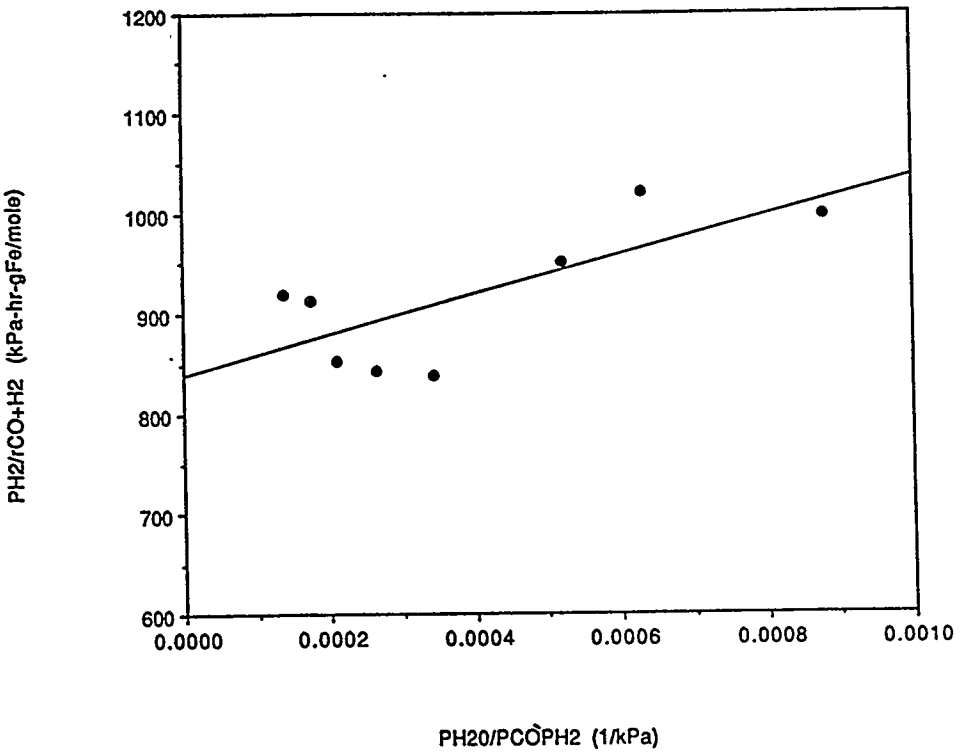

Figure IX.F-17. Test for reaction rate expression (Equation (2)) given in its linearized form by Equation (17).

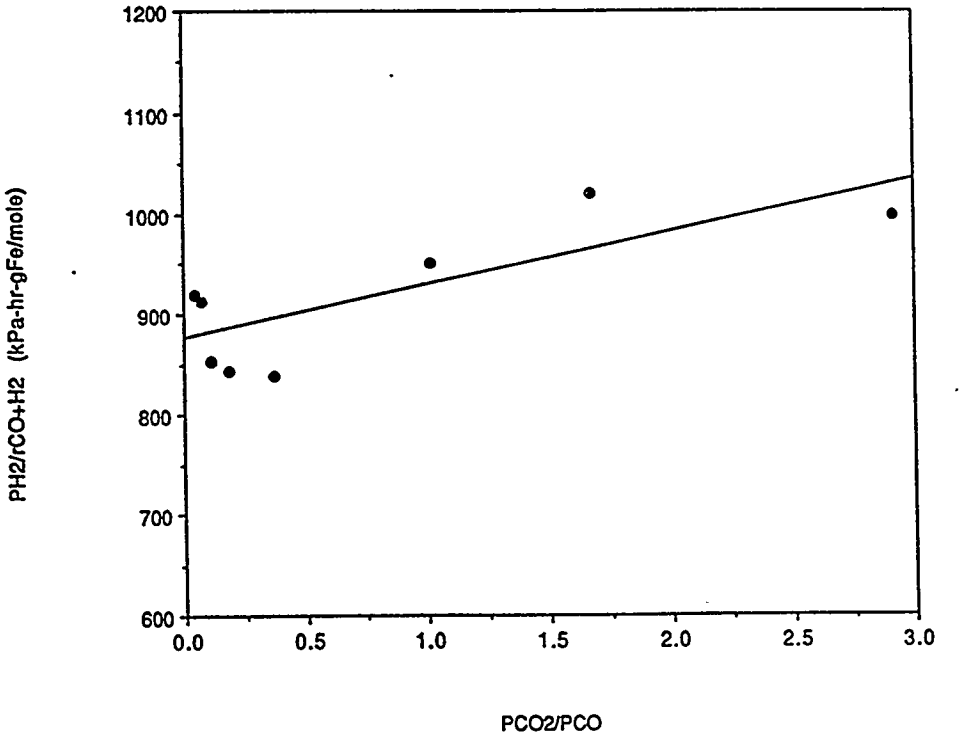

Figure IX.F-18. Test for reaction rate expression (Equation (3)) given in its linearized form by Equation (18).

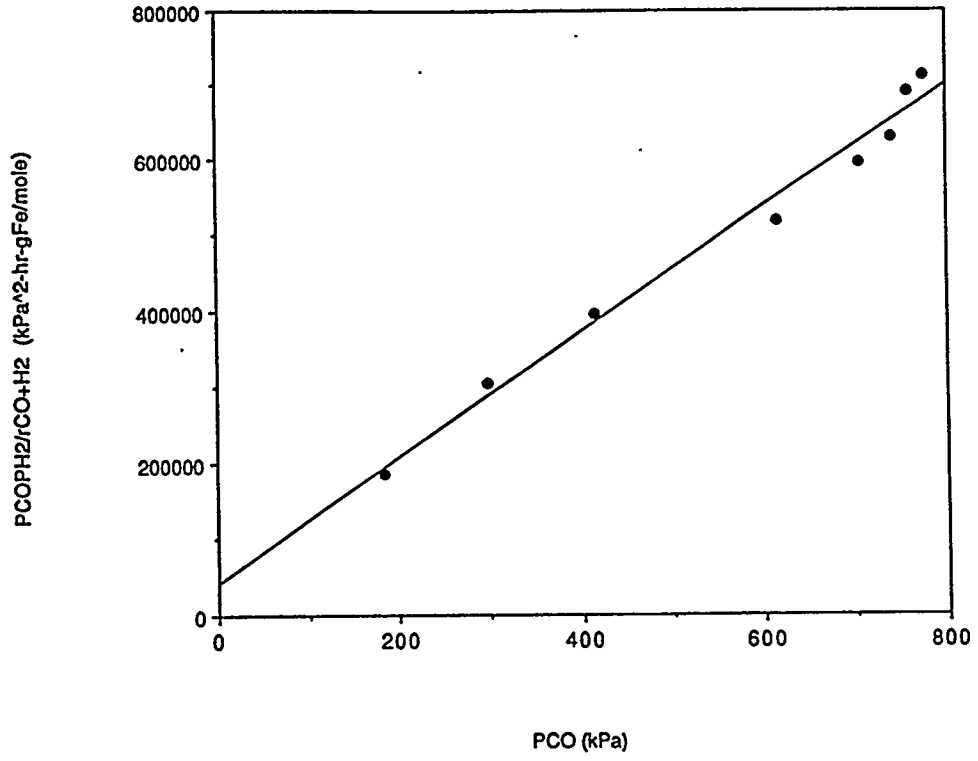

Figure IX.F-19. Test for reaction rate expression developed (Equation (19)) given in its linearized form by Equation (20).

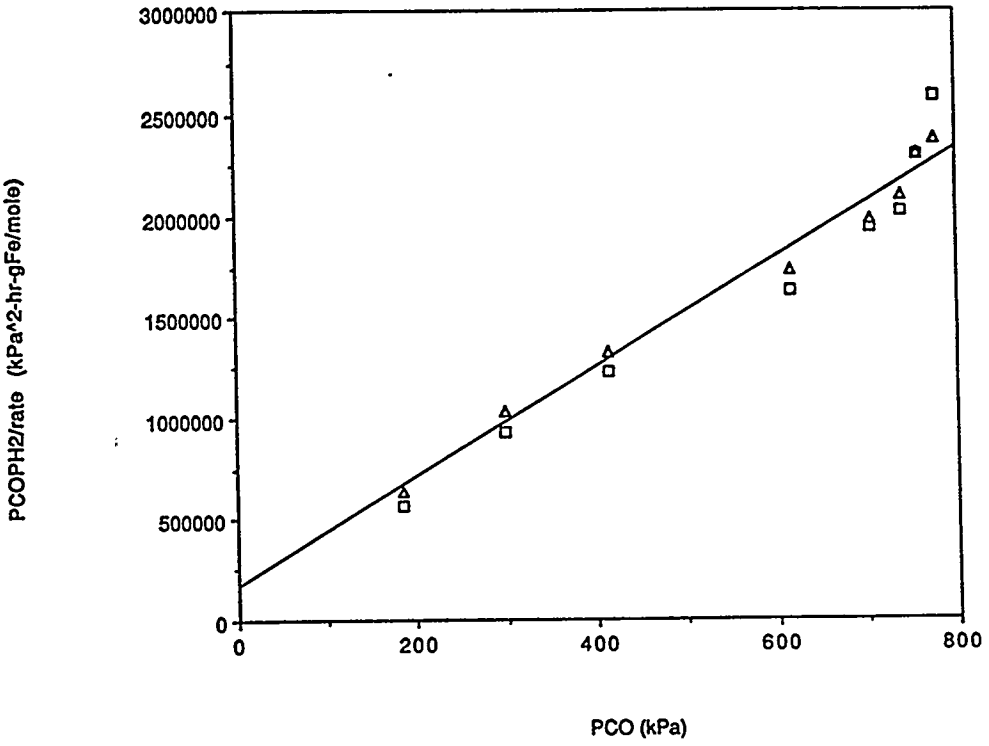

Figure IX.F-20. Test for reaction rate expression (Equation (21)) for the Fischer-Tropsch reaction.

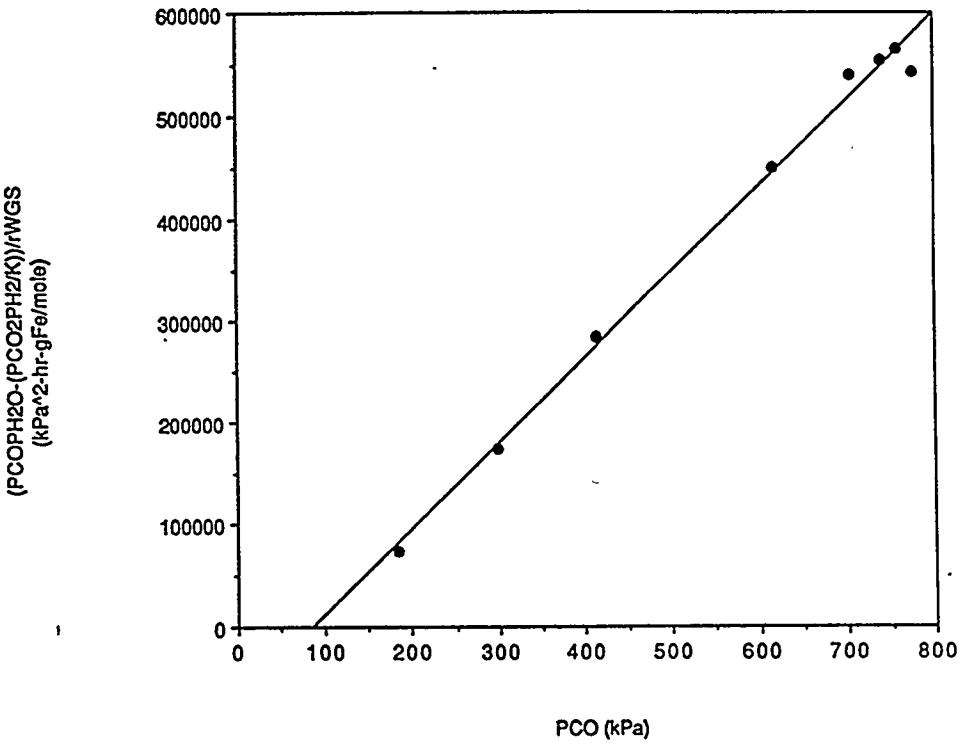

Figure IX.F-21. Test for reaction rate expression (Equation (22)) for the water gas shift reaction given in its linearized form by Equation (23).

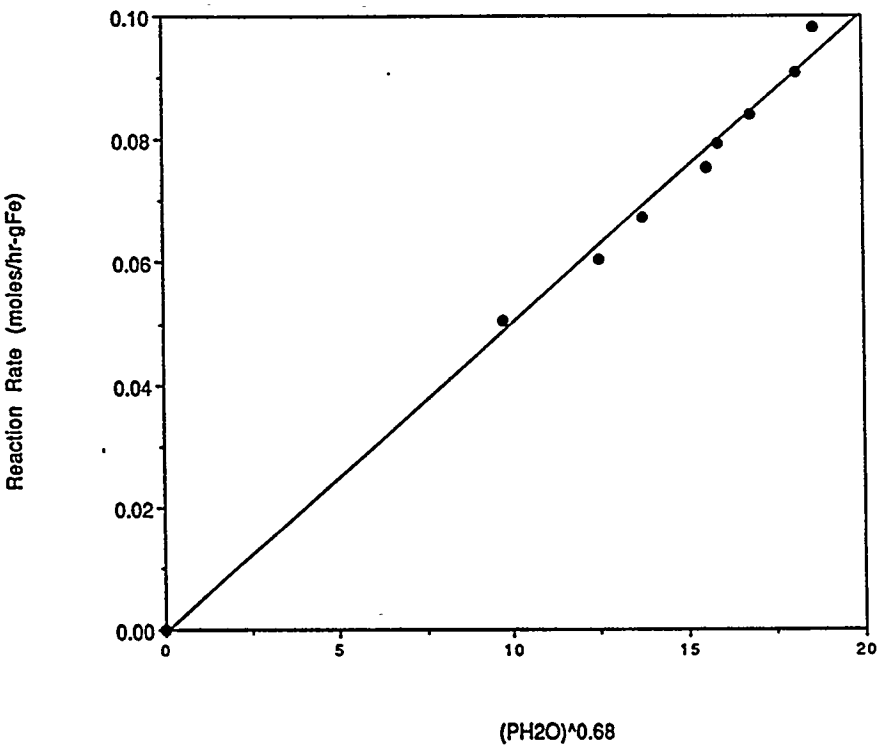

Figure IX.F-22. Test for reaction rate expression (Equation (25)) for the water gas shift reaction.